PASJ: Publ. Astron. Soc. Japan **53**, 1–6 (2001)

Substructures Revealed by the Sunyaev–Zel'dovich Effect at 150 GHz in a High-Resolution Map of RX J1347−1145

Eiichiro KOMATSU,[1,2] Hiroshi MATSUO,[3] Tetsu KITAYAMA,[4] Makoto HATTORI,[2] Ryohei KAWABE,[5] Kotaro KOHNO,[5] Nario KUNO,[5] Sabine SCHINDLER,[6] Yasushi SUTO,[7,8] and Kohji YOSHIKAWA[9]

[1] *Department of Astrophysical Sciences, Princeton University, Princeton, NJ 08544, USA*
E-mail(EK): komatsu@astro.princeton.edu
[2] *Astronomical Institute, Tôhoku University, Aoba, Sendai 980-8578*
[3] *National Astronomical Observatory, Mitaka, Tokyo 181-8588*
[4] *Department of Physics, Tokyo Metropolitan University, Hachioji, Tokyo 192-0397*
[5] *Nobeyama Radio Observatory, Minamimaki, Minamisaku, Nagano 384-1305*
[6] *Astrophysical Research Institute, Liverpool John Moores University, Byrom Street, Liverpool, L3 3AF, England, UK*
[7] *Department of Physics, The University of Tokyo, Tokyo 113-0033*
[8] *Research Center for the Early Universe, School of Science, The University of Tokyo, Tokyo 113-0033*
[9] *Department of Astronomy, Kyoto University, Kyoto 606-8502*

(Received 2000 June 20; accepted 2000 November 8)

Abstract

We report on mapping observations toward the region of the most luminous X-ray cluster, RX J1347−1145 ($z = 0.45$), through the Sunyaev–Zel'dovich effect at 21 GHz and 150 GHz with the Nobeyama 45-m telescope. While a low angular resolution image at 21 GHz (beam-size $\sigma_{\rm FWHM}$ of $76''$) shows a consistent feature with the ROSAT/HRI X-ray image, a higher angular resolution image ($\sigma_{\rm FWHM} = 13''$) at 150 GHz reveals complex morphological structures of the cluster region, which cannot be simply described by the spherical isothermal β-model. If such inhomogeneous morphological features prove to be generic for high-redshift clusters, distance measurements to the clusters based on their Sunyaev–Zel'dovich data with low angular resolution imaging should be interpreted with caution.

Key words: cosmic microwave background — cosmology: observations — distance scale — galaxies: clusters: individual (RX J1347−1145) — X-rays: galaxies

1. Introduction

A multi-band observation of galaxy clusters up to $z \sim 1$ provides a unique opportunity to reconstruct the clustering evolution, the cosmological parameters, and the peculiar velocity field on large scales (e.g., Bahcall 1988; Rephaeli 1995; Birkinshaw 1999). In particular, the recent mapping observations of clusters using state-of-the-art interferometers (Carlstrom et al. 1996, 2000) are accumulating impressive *negative* intensity images in the centimeter bands through the Sunyaev–Zel'dovich (SZ) effect (Zel'dovich, Sunyaev 1969). The most important cosmological application of such data is to estimate the global value of the Hubble constant, H_0. Although the SZ effect can be used as a potential standard candle, previous attempts to estimate H_0 were not sufficiently accurate (e.g., Kobayashi et al. 1996; Birkinshaw 1999). This is probably because they usually neglect the non-sphericity, substructure, and non-isothermal profile of the intra-cluster matter. Recent numerical simulations of clusters (e.g., Inagaki et al. 1995; Yoshikawa et al. 1998; Jing, Suto 2000) have shown that the departure from the spherical isothermal β-model is appreciable and that the inhomogeneous morphology is quite generic.

High angular resolution imaging through the SZ effect is essential in resolving the detailed structure of clusters. In centimeter interferometric measurements, a beam-size of $\sigma_{\rm FWHM} \sim 100''$ is typical, and can be as small as $\sim 40''$ (Carlstrom et al. 1996), while the brightness sensitivity is degraded. In the millimeter and submillimeter bands, on the other hand, sensitive higher resolution imaging is now feasible with bolometer array detectors. This observing technique has been successfully applied to the brightest X-ray cluster RX J1347−1145 ($z = 0.451 \pm 0.003$) at 350 GHz with $\sigma_{\rm FWHM} = 15''$ (Komatsu et al. 1999), and subsequently at 143 GHz with $\sigma_{\rm FWHM} = 23''$ (Pointecouteau et al. 1999).

The bolometric X-ray luminosity of this cluster is exceptionally high, $L_{\rm X} h_{50}^2 = 2 \times 10^{46}$ erg s^{-1} (Schindler et al. 1997), where h_{50} is the Hubble constant in units of 50 km s^{-1} Mpc^{-1}. Throughout this paper, we use $\Omega_0 = 1$ and $\lambda_0 = 0$ for simplicity. The ASCA observation implies that the emission-weighted temperature is $k_{\rm B}T_{\rm e} = 9.3^{+1.1}_{-1.0}$ keV (Schindler et al. 1997). Applying the spherical isothermal β-model to the latest ROSAT/HRI data, we obtained the central electron number density, $n_{\rm e0}h_{50}^{-1/2} = 0.093 \pm 0.004$ cm^{-3}, the core radius, $\theta_{\rm c} = 8''\!.4 \pm 1''\!.0$, and $\beta = 0.57 \pm 0.02$, where the quoted errors are at the 90% confidence levels. The total mass inferred from the hydrostatic equilibrium is $M(< 2\ h_{50}^{-1}$ Mpc$) = 1 \times 10^{15}\ h_{50}^{-1}\ M_\odot$. This cluster does not follow the temperature–luminosity relation because of the extremely high luminosity (Schindler 1999), and is known to be a strong cooling-flow cluster (Schindler et al. 1997; Allen, Fabian 1998). In this sense, this cluster may not be typical, but is an interesting target to be studied in detail individually.

The above two attempts to map the cluster using the SZ effect are not sufficiently sensitive to resolve detailed structures; the former data (Komatsu et al. 1999) are very noisy because of the bad weather condition, and the latter (Pointecouteau et al. 1999) mapped only the central narrow stripe of the cluster. Therefore, as a part of the multi-band observing project of RX J1347−1145, we carried out a SZ mapping observation of the cluster at 21 GHz and 150 GHz with the Nobeyama 45-m telescope. In this paper, we report on the complex morphological structures detected in the 150 GHz map with an unprecedented angular resolution ($\sigma_{\rm FWHM} = 13''$), which can hardly be identified from the lower resolution map at 21 GHz ($\sigma_{\rm FWHM} = 76''$). This demonstrates the importance of the high angular resolution imaging of clusters through the SZ effect.

2. Sunyaev–Zel'dovich Mapping Observations

2.1. *Centimeter Mapping at 21 GHz*

Mapping observations at 21 GHz were carried out during 2000 February 16–27 and April 14–22, in a raster-scan mode using the dual circular polarization HEMT amplifier mounted on the Nobeyama 45-m telescope. In total, 9 scans were performed along the two orthogonal directions, and each scan was separated by $40''$, yielding a final field-of-view of $6' \times 6'$. A reference beam position was set to be $400''$ away from a main beam, and the beam-size, $\sigma_{\rm FWHM} = 76''\!.5$, was estimated by observing 3C 279. The beam was accurately fitted to a Gaussian. The total exposure time per field-of-view amounted to 31.2 ks in February and 32.1 ks in April. Since 81 pixels ($40'' \times 40''$ each) were independent in the field-of-view, these exposure times correspond to 385 s and 396 s per pixel, respectively.

The system noise temperatures were typically 135 K in February and 185 K in April. The atmospheric absorption was corrected in real time by a chopper-wheel method assuming that the atmospheric temperature was the same as the calibration load at ambient temperature. The ambient temperature was monitored continuously during the observation. The optical depth at 21 GHz was typically less than 0.04.

We calibrated the primary flux using 3C 286 (2.56 ± 0.02 Jy; Ott et al. 1994). Because our detector measures circularly polarized light, the linear polarization of 3C 286 does not affect an accuracy of flux calibration. The stability of the antenna efficiency was tracked by monitoring the pointing source (1334−127); we found that the system was so stable that the r.m.s. variation in peak flux was 2% in February and 3% in April throughout the entire observation. We corrected this small variation for each observing run according to the pointing data observed immediately before and after each run. We conservatively adopted 3% peak flux variation in April as a calibration error. The pointing offset was negligible compared with the beam-size.

We subtracted the low-frequency scanning-noise from the map on the basis of the PLAIT method (Emerson, Gräve 1988) with a scale-length half the scan-length. The resulting 1σ noise-levels in images were 1.3 mJy beam^{-1} in February and 1.7 mJy beam^{-1} in April. Combining the February and April runs, the final image achieved a noise-level of 0.9 mJy beam^{-1}.

2.2. *Millimeter Mapping at 150 GHz*

A higher angular-resolution mapping of the cluster was performed with the Nobeyama Bolometer Array (NOBA; Kuno et al. 1993) on 1999 March 16 (20 ks) and April 15 (8.5 ks), as well as during 2000 February 16–27 (52.7 ks). The total integration time was 81.2 ks. Since 441 pixels ($5''\!.3 \times 5''\!.3$ each) were independent in the field-of-view, it corresponds to 184 ks per pixel.

NOBA consists of seven bolometers in a hexagonal pattern with their band-passes centered at 150 GHz and bandwidths of 30 GHz. Bolometers are read-out through six differential circuits between a central bolometer and the other six surrounding ones. Fluctuations in atmospheric emissions are subtracted in real time by the read-out electronics. Beam switching, or sky chopping, is not used. The observation of this cluster was made with raster scans. A position angle of the array to the scan direction was $19^\circ\!.1$. A single raster scan yielded seven scan paths separated by $5''\!.3$ each, and an observing stripe of $37''\!.1$ in width. Three stripes thus covered a field-of-view of $1'\!.9 \times 1'\!.9$ in right ascension and declination. Image restoration was performed using the six differential signals.

At the beginning and the end of each observing day, an elevation scan was made to measure the atmospheric transparency. The measured zenith optical depths at

150 GHz were 0.094–0.15 and 0.065–0.098 in our 1999 and 2000 runs, respectively. These scan data were also used to correct different sensitivities among bolometers down to a few percent accuracy. A pointing observation was made every 0.5 to 1 hr, depending on the weather condition. The variation in the pointing was usually within $3''$. The data taken under strong wind conditions were discarded because of the unstable pointing and the degraded antenna efficiency.

We calibrated the primary flux using the Mars in 1999, and K3-50A and OH5.89-0.39 in 2000. The flux of Mars was obtained with the FLUXES procedure in the STARLINK package, and we employed 6.5 ± 0.2 Jy (Sandell 1994) and 8.8 ± 0.9 Jy (Falcke et al. 1998) for the fluxes of K3-50A and OH5.89-0.39, respectively. The beam pattern was measured using 3C 279, which yielded $\sigma_{\rm FWHM} = 12''\!.5$ and $13''\!.2$ in 1999 and 2000, respectively. The uncertainty of the beam-size was as large as $1''$. The beam was slightly elongated along the elevation direction by $\sim 10\%$, and the side-lobe level amounted to 3% of the peak value, whereas the Gaussian yielded 1% of the peak value. The side-lobe levels of the bolometers varied within a few percent. The pointing and gain stabilities were checked using 1334−127, and the r.m.s. variations in the peak fluxes were 12% in 1999 and 14% in 2000. These variations are largely ascribed to a strong elevation-dependence of the antenna efficiency at 150 GHz. After correcting this gain variation, we estimated the total calibration error to be 11% (7% in 1999 and 14% in 2000). The larger error in 2000 was due to the fact that the flux of 1334−127 daily changed by up to $\sim 20\%$ probably because of the burst, while it was stable in the 1999 run.

Spike noise above the 4σ level appearing in time-ordered data were removed. Again, the map was created using the PLAIT method; the 1σ noise-level in the final image was 1.6 mJy beam^{-1} (2.4 mJy beam^{-1} in 1999, and 2.1 mJy beam^{-1} in 2000). In the final map, the averaged flux at the edge of the map ($64''$ away from the center), 0.50 ± 0.15 mJy beam^{-1}, was subtracted to define the zero-level of the data.

3. Results

3.1. Low Angular Resolution Image at 21 GHz

Figure 1a displays the final map of RX J1347−1145 at 21 GHz, which shows a bright point source near to the center of the cluster. In order to accurately estimate the position and flux at 21 GHz, we observed the source with VLA at 8.46 GHz (18 ks) on 1999 May 16, and at 22.46 GHz (3.6 ks) on 1999 May 20. The measured fluxes were 22.42 ± 0.04 mJy at 8.46 GHz and 11.55 ± 0.17 mJy at 22.46 GHz. Since the VLA configuration was insensitive to the SZ effect, these values accurately measured the central radio source flux. The derived source position is ($13^{\rm h}47^{\rm m}30^{\rm s}\!.622 \pm 0^{\rm s}\!.0005$, $-11^\circ45'09''\!.44 \pm 0''\!.009$), and precisely coincides with that of the optical center of the central cD galaxy. Although the X-ray peak position from the ROSAT/HRI data is offset from the optical center (Schindler et al. 1997), this offset is smaller than the nominal pointing uncertainty of ROSAT/HRI. In the following discussion, therefore, the X-ray peak position is assumed to coincide with the optical center and the central radio source position.

In total, we obtained three datasets at 21 GHz taken during three years: 1998 March (Komatsu et al. 1999), 1999 March (unpublished), and 2000 February and April (this paper). The 1998 and 1999 runs were conducted in the cross-scan mode. We measured central peak-intensities of 8.6 ± 2.0 mJy beam^{-1} in 1998, 7.8 ± 1.2 mJy beam^{-1} in 1999, and 8.3 ± 0.9 mJy beam^{-1} in 2000. These results show no significant time variation of the source flux value during the past two years, and the averaged peak-intensity was 8.2 ± 0.7 mJy beam^{-1}.

Figure 1b plots the 21 GHz map after subtracting the contribution of the point source, adopting the VLA flux at 22.46 GHz. On the larger scale structure of the negative brightness distribution than the sampling resolution of $40''$, its overall shape around the central part is fairly similar to that of the X-ray surface brightness contours overlaid in white solid lines, i.e., elongating along the north–south direction, supporting the SZ interpretation over the entire cluster scale.

The resulting central intensity (smoothed over the beam-size) of the SZ decrement relative to the edge of map ($200''$ away from the center) is $I_{\rm SZ}(0) = -3.3 \pm 0.9$ mJy beam^{-1}, or equivalently, $\Delta T_{\rm RJ}(0) = -1.6 \pm 0.4$ mK in terms of the Rayleigh–Jeans brightness temperature decrement. Deconvolving the beam-pattern by approximating the cluster profile with the spherical isothermal β-model with the ROSAT/HRI best-fit values for $\theta_{\rm c}$ and β (section 1), we obtained the intrinsic SZ brightness temperature decrement, $\Delta T_{\rm RJ}^{\rm intrinsic}(0) = \Delta T_{\rm RJ}(0)/0.38 = -4.2 \pm 1.0$ mK, and then the central y-parameter, $y(0) = (7.8 \pm 2.1) \times 10^{-4}$ (relative to the edge of map). Moreover, if we average the measured peak-intensities over the datasets taken during three years, we obtain $y(0) = (7.7 \pm 1.6) \times 10^{-4}$.

Our $y(0)$ agrees very well with the value expected from the X-ray best-fit parameters, $y(0)h_{50}^{1/2} = 8.0 \times 10^{-4}$, if the SZ effect is negligible at the edge of the map. Note that Komatsu et al. (1999) possibly overestimated the SZ intensity at the cluster center by 1.75 mJy beam^{-1}, because they used the central source flux of 13.3 mJy at 21 GHz based on the power-law interpolation of the spectrum at 1.4, 28.5, and 100 GHz. We now realize that it is not a good approximation.

3.2. *High Angular Resolution Image at 150 GHz*

Figure 1c shows the image at 150 GHz smoothed with a Gaussian filter so that the effective beam-size becomes $20\farcs6$ (the 1σ noise-level is 1.3 mJy beam^{-1}). Although the central point source is fainter at 150 GHz than at 21 GHz, it still affects the diffuse negative intensity field around the center to some extent. The most remarkable feature in this image is a strong negative intensity region located $\sim 20''$ south–east from the center. The peak intensity in this region is -5.4 mJy beam^{-1} relative to the edge of the map. This value is at the 4.2σ significance level, and is 2.5-times larger than that expected from the spherical isothermal β-model, $I_{\rm SZ}(\Delta\theta = 20'') \sim -2$ mJy beam^{-1}.

In the following, we quantify the statistical significance of the detection of this negative excess emission. As shown in figure 2, we divide the data into four regions: south–east (SE), south–west (SW), north–east (NE), and north–west (NW). The central region is excluded so as to remove any contamination of the point source. We then evaluated the fluxes in those regions. The results are summarized in table 1 together with the 1σ error of 2.0 mJy each. The mean flux averaged over all regions is -6.4 ± 1.0 mJy relative to the edge of the map, and thus the detection of the SZ decrement at 150 GHz is 6.4σ level. The reality of the negative excess in the SE region is supported by the following facts: (i) the fluxes of the other three regions are consistent with each other within the 1σ level, (ii) relative to the mean flux over the other three regions, $\bar{F} = -4.7 \pm 1.15$ mJy, the excess flux in the SE region is $F_{\rm SE} - \bar{F} = -6.6 \pm 2.3$ mJy, corresponding to 2.9σ significance, and (iii) the excess in the SE region is persistent both in 1999 and in 2000. Thus, we interpret this negative excess flux as being due to an enhanced SZ effect.

To further explore the significance of this excess, let us consider the residual map after subtracting the SZ signal, while assuming the spherical isothermal β-model. For this purpose, we employed the best-fit radial profile from the ROSAT/HRI data, and the emission-weighted temperature, 9.3 keV, measured with ASCA (section 1). We refer to this as model L (low temperature). After convolving the model image with the effective beam and correcting for the zero-level, we subtracted this from the observed map. We then found that the model L implies a central radio source flux of 3.8 ± 1.3 mJy, and the expected flux in each region is -5.1 mJy. The latter value is consistent with those listed in table 1, except for the SE region where the difference is 3.1σ. This is also consistent with the mean flux, indicating that the global feature of the SZ effect at 150 GHz is consistent with model L as well as at 21 GHz. Figure 1d shows the 150 GHz map after subtracting the central source flux of 3.8 mJy. While the X-ray contours overlaid in the figure seem to trace the detected SZ enhancement to some extent, the X-ray flux in the SE region is much smaller than that expected from the excess SZ flux which we detected at 150 GHz.

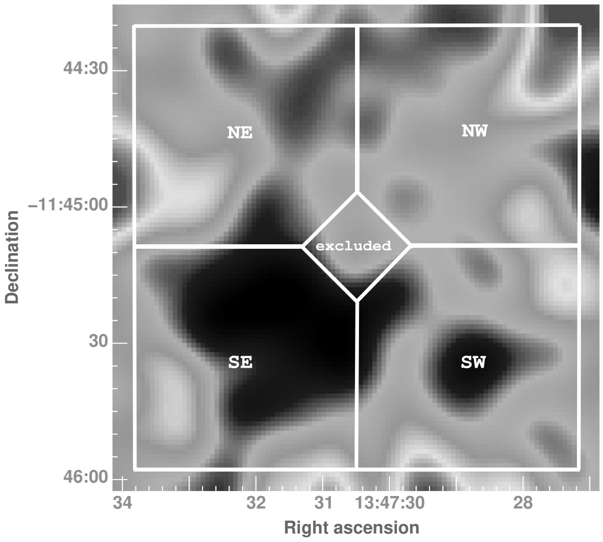

Fig. 2.. Definition of regions (see subsection 3.2).

Table 1. Fluxes in four regions toward RX J1347−1145 (see figure 2 for the definition). All values are evaluated relative to the edge of the map (64″ away from the center). Models L and H represent the expected fluxes from the spherical isothermal β model with temperatures of $k_{\rm B}T_{\rm e} = 9.3$ keV and 16.2 keV, respectively.

	flux [mJy]
SE (south-east)	-11.3 ± 2.0
NE (north-east)	-4.7 ± 2.0
NW (north-west)	-3.3 ± 2.0
SW (south-west)	-6.1 ± 2.0
mean	-6.4 ± 1.0
model L (9.3 keV)	-5.1
model H (16.2 keV)	-8.8

In summary, we conclude that we detected an inhomogeneous morphology of the SZ signal toward the cluster at 150 GHz. The angular scale of the negative excess is around $40''$, and thus cannot be resolved in the lower angular resolution image at 21 GHz.

4. Comparison with Previous Work

Using the IRAM/Diabolo bolometer array, Pointecouteau et al. (1999) found that the peak position of the SZ decrement at 143 GHz is offset to the east of the X-ray peak position. Since they scanned in a narrow strip ($30''$ in declination and $120''$ in right ascension) along west–east direction, whose width was comparable to the beam-size ($\sigma_{\rm FWHM} = 23''$), the resulting map is insensitive to the offset in north–south direction. Thus, their result does not contradict our finding on the image basis. They presented a different interpretation for this negative enhancement; they assumed that the offset between the X-ray peak position and the radio source position is real, and ascribed the offset between the SZ and the X-ray peak positions to contamination of the positive radio source embedded in the SZ decrement tracing the X-ray signal. More specifically, they found the best-fit values for the central y-parameter, $y(0) = 12.7^{+2.9}_{-3.1} \times 10^{-4}$, and for the central point source flux, $6.1^{+4.3}_{-4.8}$ mJy, at 143 GHz, adopting the β-model radial profile from the X-ray data. This $y(0)$ corresponds to a much higher temperature of 16.2 keV than the ASCA value. We call this set of parameters model H (high temperature). When subtracting the SZ flux of the model H from our map at 150 GHz, we find a central source flux of 6.6 ± 1.3 mJy. Since this value is close to their fit, our data at 150 GHz are consistent with their data, apart from the interpretation.

Here, we compare our data to theirs quantitatively. (i) Taking into account a relativistic correction to the SZ effect (Itoh et al. 1998) to extrapolate their $y(0)$ at 143 GHz into the value at 21 GHz, model H predicts $y(0) = 13.9^{+3.2}_{-3.4} \times 10^{-4}$ at 21 GHz. This value significantly exceeds our observed value, $(7.7 \pm 1.6) \times 10^{-4}$, which is consistent with model L. (ii) Model H predicts a flux of -8.8 mJy for each region defined in figure 2, which is systematically smaller than our observed values listed in table 1. Therefore, we conclude that model L with the excess SZ effect is more consistent with our data at 21 GHz and 150 GHz data than model H. Their higher value of $y(0)$ than ours is probably because of their narrower field-of-view. The excess SZ effect detected in the SE region would dominate the mean signal in their map, resulting in an overestimate of $y(0)$.

Incidentally, the negative flux in the SE region at 150 GHz should show up as a *positive* SZ flux of 11 mJy in the JCMT/SCUBA band (350 GHz). While Komatsu et al. (1999) did not identify the corresponding peak in their SCUBA map, this is not inconsistent one another because of the high noise-level in their SCUBA map ($1\sigma = 8$ mJy beam^{-1}).

5. Discussion

Possible physical explanations for the origin of the excess SZ feature include a) a projection contamination of another higher redshift cluster, b) warm gas associated with large-scale filamental structures, c) a substructure in the cluster gas, d) a cooling flow around the central region, and e) non-gravitational heating from AGNs and/or supernovae. Actually, any explanation needs to be somewhat contrived, because it should be simultaneously consistent with the fairly smooth X-ray brightness distribution. Specifically, a) requires that the background cluster should be at $z > 3$, b) is viable only if the low temperature (~ 0.4 keV) gas extends over 1 Gpc along the line of sight, c) implies that the temperature of the substructure is larger than ~ 100 keV, and d) and e) indicate that either pressure or virial equilibrium of the intracluster gas should be abandoned. Thus, none of those possibilities seems to be sufficiently satisfactory.

Nevertheless, if the complex morphological structure is generic to other high-redshift clusters, distance measurements to the clusters based on the SZ data should be interpreted with caution. To elucidate this, let us consider how the enhanced decrement region at 150 GHz systematically affects the estimate of the Hubble constant from the 21 GHz data. The excess SZ flux at 21 GHz in the SE region is expected as -0.43 mJy, based on the deviation from model L at 150 GHz in the same region (-6.2 mJy). Since the extent of the SE region is smaller than the beam-area at 21 GHz, this flux amounts to 13% of $I_{\rm SZ}(0)$ at 21 GHz. This corresponds to overestimating $I_{\rm SZ}(0)$ relative to the isothermal β-model prediction, and thus to a systematic underestimate of H_0 by 22% through the relation $H_0 \propto I_{\rm SZ}^{-2}(0)$. This consideration might be relevant to understanding the Hubble diagram from the SZ effect (e.g., Kobayashi et al. 1996; Birkinshaw 1999).

As demonstrated here, single-dish measurements of the SZ effect with high angular resolution play a complementary role to interferometers in exploring the intracluster gas state. In addition, a more accurate and higher resolution imaging observation in X-ray band with Chandra and XMM–Newton observatories is important to understand the physical processes in this cluster as well as the future follow-up SZ observations including the SZ dedicated interferometers and JCMT/SCUBA.

We thank Akihiro Sakamoto and the NRO staff for their help during the observation at NRO, Izumi Ohta for observing RX J1347−1145 with NMA, and Wolfgang Reich for providing the data of OH5.89-0.39 and for useful comments on the data analysis. We also thank John Carlstrom, Uroš Seljak, and David N. Spergel for many valuable comments which have improved this paper. E.K., T.K. and K.Y. acknowledge fellowships from Japan Society for the Promotion of Science. This research was supported in part by the Grants-in-Aid for the Center-of-Excellence (COE) Research of the Ministry of Education, Science, Sports, and Culture of Japan to RESCEU (No. 07CE2002), and Grand-in-Aid of the Ministry of Education, Sports, and Culture of Japan (No. 11440060).

References

Allen, S. W., & Fabian, A. C. 1998, MNRAS, 297, L57
Bahcall, N. A. 1988, ARA&A, 26, 631
Birkinshaw, M. 1999, Phys. Rep., 310, 97
Carlstrom, J. E., Joy, M. K., & Grego, L. 1996, ApJ, 456, L75

Carlstrom, J. E., Joy, M. K., Grego, L., Holder, G. P., Holzapfel, W. L., Mohr, J. J., Patel, S., & Reese, E. D. 2000, Physica Scripta, T85, 148
Emerson, D. T., & Gräve, R. 1988, A&A, 190, 353
Falcke, H., Goss, W. M., Matsuo, H., Teuben, P., Zhao, J. H., & Zylka, R. 1998, ApJ, 499, 731
Inagaki, Y., Suginohara, T., & Suto, Y. 1995, PASJ, 47, 411
Itoh, N., Kohyama, Y., & Nozawa, S. 1998, ApJ, 502, 7
Jing, Y. P., & Suto, Y. 2000, ApJ, 529, L69
Kobayashi, S., Sasaki, S., & Suto, Y. 1996, PASJ, 48, L107
Komatsu, E., Kitayama, T., Suto, Y., Hattori, M., Kawabe, R., Matsuo, H., Schindler, S., & Yoshikawa, K. 1999, ApJ, 516, L1
Kuno, N., Matsuo, H., Mizumoto, Y., Lange, A. E., Beeman, J. W., & Haller E. E. 1993, Int. J. Infrared Millimeter Waves, 14, 749
Ott, M., Witzel, A., Quirrenbach, A., Krichbaum, T. P., Standke, K. J., Schalinski, C. J., & Hummel, C. A. 1994, A&A, 284, 331
Pointecouteau, E., Giard, M., Benoit, A., Désert, F. X., Aghanim, N., Coron, N., Lamarre, J. M., & Delabrouille, J. 1999, ApJ, 519, L115
Rephaeli, Y. 1995, ARA&A, 33, 541
Sandell, G. 1994, MNRAS, 271, 75
Schindler, S. 1999, A&A, 349, 435
Schindler, S., Hattori, M., Neumann, D. M., & Böhringer, H. 1997, A&A, 317, 646
Yoshikawa, K., Itoh, M., & Suto, Y. 1998, PASJ, 50, 203
Zeldovich, Ya. B., & Sunyaev R. A. 1969, Ap&SS, 4, 301

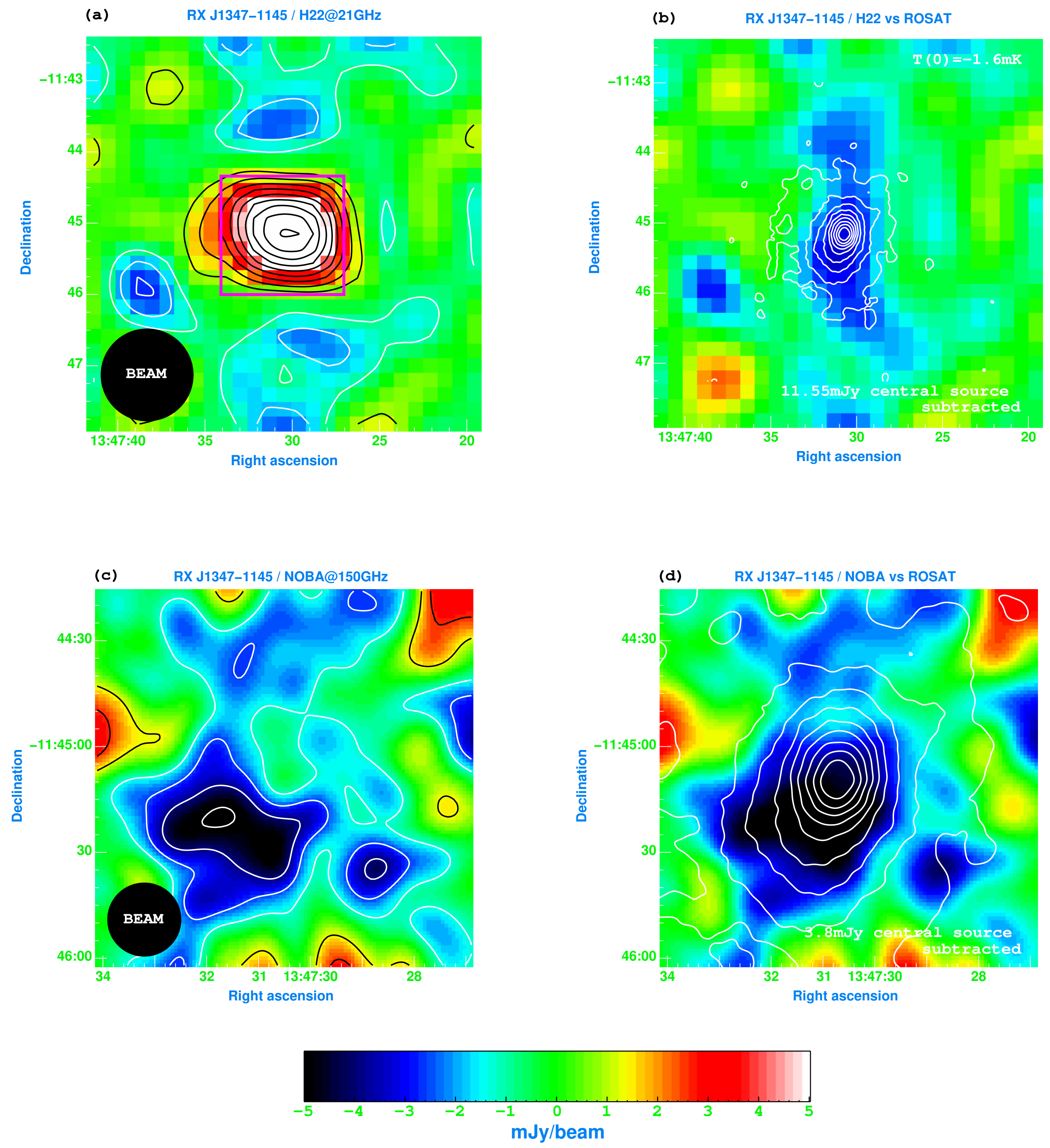

Fig. 1.. SZ maps of RX J1347−1145. (a) the 21 GHz map before subtracting the central point source. Field-of-view is $6' \times 6'$ (2.4 h_{50}^{-1} Mpc × 2.4 h_{50}^{-1} Mpc). The black (white) lines represent 1σ contours of positive (negative) intensities, where $1\sigma = 0.9$ mJy beam^{-1}. The beam-size is shown as a filled black circle having a diameter of $76''\!.5$. The area defined by a magenta solid line corresponds to (c) and (d). (b) the 21 GHz map after subtracting the central point source. We used the VLA flux of 11.55 mJy. Overlaid in white lines are the X-ray contours, which represent 10–90% of the peak value in 10% intervals. The equivalent Rayleigh–Jeans temperature at the center is $\Delta T_{\rm RJ}(0) = -1.6 \pm 0.4$ mK. (c) the 150 GHz map before subtracting the central point source. The field-of-view is $1'\!.9 \times 1'\!.9$ (0.75 h_{50}^{-1} Mpc × 0.75 h_{50}^{-1} Mpc). The lines have the same meaning as in the panel (a). In this panel, the beam-size is $20''\!.6$, and $1\sigma = 1.3$ mJy beam^{-1}. (d) the 150 GHz map after subtracting the central point source (assuming the flux of 3.8 mJy) overlaid with the X-ray contours.